https://doi.org/10.7840/kics.2025.50.11.1687

Spot Beam Power Optimization for an Energy Efficient Multi-LEO Satellite Network

Jihwan Moon◆, Hoon Lee°

ABSTRACT

This paper proposes a spot beam power control method for downlink non-terrestrial networks consisting of multiple low Earth orbit (LEO) satellites. Each designated ground access point (GAP) is continuously served by a steering beam from LEO satellites during their visibility period. We address the global energy efficiency (GEE) maximization task to determine the optimal tradeoff between the sum-rate and total power consumption of LEO satellites. The GEE maximization problem is formulated by taking the inter-beam, inter-carrier, and terrestrial network interference into account. To ease the complexity of the problem, we further simplify the expressions of the GEE and interference and then propose a successive convex approximation (SCA)-based spot beam power optimization method. Numerical results validate its effectiveness over baseline algorithms in different system setups.

Key Words : Satellite communications, non-terrestrial network, low earth orbit, energy efficiency, power optimization

Ⅰ. Introduction

The rapid evolution of wireless communications technologies has led to an increased focus on a non-terrestrial network (NTN) as a means to achieve global connectivity[1]. It is considered to be integral to the vision of ubiquitous coverage, especially in remote and underserved regions, beyond existing traditional terrestrial infrastructures for the upcoming sixth-generation (6G) standard[2]. Consequently, a vast number of researchers have begun to pay attention to addressing the unique challenges of NTNs[3].

Fundamental challenges in the management tasks of NTNs include propagation delays between satellites and ground access points (GAPs) and Doppler shifts stemming from the movement of satellites[4]. This entails the development of advanced optimization techniques tailored for NTNs. The integration of NTNs with terrestrial networks was explored in [5], emphasizing the role of beamforming and artificial intelligence technologies. The authors in [6] highlighted challenges in satellite beamforming and inter-satellite transmissions for radio resource management, mobility management, and dynamic network slicing. Also, [7] evaluated various multi-layered NTNs, offering guidelines on achieving a balance between system flexibility and network performance with coverage and latency constraints into consideration.

※ This work was supported in part by Korea Research Institute for defense Technology planning and advancement(KRIT) grant funded by the Korea government(DAPA(Defense Acquisition Program Administration)) (KRIT-CT-22-047, Space-Layer Intelligent Communication Network Laboratory, 2022), in part by the IITP(Institute of Information & Coummunications Technology Planning & Evaluation)-ITRC(Information Technology Research Center) grant funded by the Korea government(Ministry of Science and ICT)(IITP-2025-RS-2024-00437886, 33%), and in part by the National Research Foundation of Korea (NRF) funded by the Ministry of Science and ICT (MSIT) Korea Government under Grants RS-2022- NR070834.
◆ First Author : Hanbat National University, Department of Mobile Convergence Engineering, anschino@staff.hanbat.ac.kr, 정회원
° Corresponding Author : Ulsan National Institute of Science and Technology (UNIST), Department of Electrical Engineering hoonlee@unist.ac.kr, 정회원
논문번호 : 202504-087-B-RU, Received April 15, 2025; Revised May 31, 2025; Accepted June 5, 2025

Meanwhile, energy efficiency has emerged as a critical performance measure in the design and operation of NTNs[8]. By optimizing power consumption, we can enhance the lifespan of satellite components and reduce operational costs. Various NTN management techniques, such as adaptive power control, energy-efficient routing algorithms, and dynamic resource allocation, have been proposed to address these challenges. In particular, [9] tackled energy efficiency maximization in multibeam satellite systems under total power and quality-of-service constraints. Precoding optimization algorithms were proposed based on zero forcing (ZF) and successive convex approximation (SCA), verified using real measured channel data. Furthermore, [10] investigated a two-step quadratic transformation method to address energy efficiency maximization in multibeam satellite communications. By converting the non-convex problem into an equivalent convex one, an alternating optimization algorithm can be derived that iteratively identifies effective networking solutions. In [11], an energy-efficient resource allocation in space-air-sea NTNs for maritime coverage was presented. A mixed-integer programming task was formulated which maximizes the system energy efficiency by jointly optimizing user equipment association, power control, and unmanned aerial vehicle (UAV) deployment. In addition, [12] maximized the global energy efficiency (GEE) of the whole NTN supporting multiple ground access points (GAPs) while accounting for various interference effects.

With the aid of machine learning, [13] assigned spreading factors (SFs) to end devices to minimize co- SF interference and enhance the energy efficiency. In addition, [14] explored the integration of open radio access network (O-RAN) within NTNs, focusing on optimizing the dynamic functional split between centralized units (CU) and distributed units (DU) to enhance energy efficiency. A deep Q-network method was employed, which dynamically determines the optimal network function split and selects the best NTN platform based on real-time conditions and traffic demands.

Most of the previous works considered a single satellite system. For this reason, these cannot scale effectively with the increasing number of satellites. To this end, our previous work[15] extended the single satellite system[12] to general multiple low Earth orbit (LEO) satellite NTNs and proposed the optimal GAP- beam assignment while assuming equal power allocation for all GAPs and beams. Such an approach has been shown to degrade the GEE performance. In particular, the GEE improvement with an increasing number of LEO satellites was marginal even though the system could exploit greater link diversity. This suggests that relying solely on GAP-beam assignment with fixed transmit power may be insufficient to effectively mitigate both inter-cell and intra-cell interference. Therefore, it is necessary to further investigate the impact of optimal downlink power control to fully leverage the benefits of multi-satellite configurations.

This paper presents an efficient algorithm for maximizing the GEE performance of multi-LEO satellite NTNs where several satellites support multiple GAPs in the downlink. We aim to optimize the spot beam power of LEO satellites considering practical challenges of NTNs such as inter-beam, inter-carrier, and terrestrial interference signals. We first construct the GEE maximization problem, which is proven to be non-convex. To handle this difficulty, the SCA technique is applied that addresses approximated convex tasks of the original non-convex GEE maximization problem. Numerical results validate the effectiveness of the proposed algorithm over baseline schemes.

Ⅱ. System Model

We consider a multi-LEO network illustrated in Fig. 1 where S satellites support K GAPs in the downlink. Each satellite projects at most M spot beams, and each GAP is assumed to be assigned to at most one spot beam. In terrestrial networks, B ground base stations (GBSs) share the same frequency spectrum with LEO satellites, e.g., Ku- or Ka-band of satellite communications and frequency range 2 of the fifth-generation (5G)[16], which interfere GAPs. The channel state information and locations of the GAPs and GBSs can be available at the satellites by the enhanced channel estimation and localization algorithms[12].

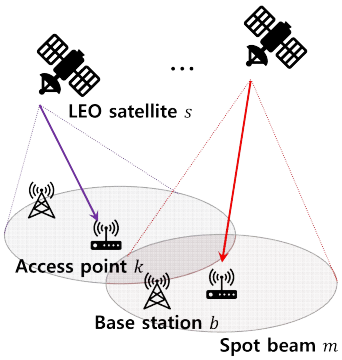

Fig. 1. System model for multi-LEO networks

The signal-to-interference-plus-noise ratio (SINR) of GAP k on spot beam m of satellite s, denoted by $\gamma_{k,m,s}$, can be expressed by

$$\gamma_{k,m,s} = \frac{G_{\mathrm{AP},k} L_{k,s} G_{\mathrm{main},s} P_{k,m,s}}{\mathrm{IBI}_{k,m,s} + \mathrm{ICI}_{k,m,s} + \sigma_{z,k}^2}, \tag{1}$$

where $G_{\mathrm{main},s}$ and $G_{\mathrm{AP},k}$ denote the main lobe antenna gain of satellite s and antenna gain of GAP k, respectively, Pk,m,s indicates the transmit power allocated to spot beam m of satellite s for GAP k, $L_{k,s}$ denotes channel attenuation between GAP k and satellite s, and $\sigma_{z,k}^2$ stands for the noise variance at GAP k. In addition, $\mathrm{IBI}_{k,m,s}$ and $\mathrm{ICI}_{k,m,s}$ account for the inter-beam interference (IBI) and inter-carrier interference (ICI) by the Doppler effect for GAP k on beam m of satellite s.

These interference terms are written by

$$\mathrm{IBI}_{k,m,s} = G_{\mathrm{AP},k} \sum_{\substack{(k',m',s') \\ \neq (k,m,s)}} L_{k,s'} G_{\mathrm{side},k,m',s'} P_{k',m',s'} x_{k',m',s'}, \tag{2}$$

$$\mathrm{ICI}_{k,m,s} = G_{\mathrm{AP},k} L_{k,s} G_{\mathrm{main},s} P_{k,m,s} \left(1 - \mathrm{sinc}^2 \left(f_{k,s} T_{\mathrm{sym}}\right)\right), \tag{3}$$

where $G_{\mathrm{side,X},m,s}$ accounts for the sidelobe antenna gain towards ground node X by beam m of satellite s, Tsym represents the symbol duration, and fk,s denotes the Doppler shift between GAP k and satellite s. Here, the Doppler shift is calculated as

$$f_{k,s} = \frac{v_s}{C} f_c \cos \phi_{k,s}, \tag{4}$$

where v_s equals the velocity of satellite s, $C = 3 \times 10^8$ m/s is the speed of light, fc stands for the carrier frequency, $C = 3 \times 108$ m/s is the speed of light, and $\phi k,s$ denotes the angle of the receiving direction of GAP k and moving direction of satellite s, respectively. Also, $x_{k,m,s} \in \{0, 1\}$ in (2) stands for a binary indicator that equals 1 if spot beam m of satellite s is assigned to GAP k and 0 otherwise. The beam assignment is assumed to be fixed such that each beam is dedicated to a single GAP and vice versa. Thus, $x_{k,m,s} \in \{0, 1\}$ is randomly chosen to satisfy

$$\sum_{s=1}^{S} \sum_{m=1}^{M} x_{k,m,s} \leq 1, \forall k = 1, \ldots, K, \tag{5}$$

$$\sum_{k=1}^{K} x_{k,m,s} \leq 1, \forall m = 1, \ldots, M \text{ and } s = 1, \ldots, S, \tag{6}$$

$$\sum_{m=1}^{M} \sum_{k=1}^{K} x_{k,m,s} \leq M, \forall s = 1, \ldots, S. \tag{7}$$

Notice that $x_{k,m,s}$ can be zero when the numbers of GAPs and beams are unequal.

Ⅲ. Problem Formulation

This section formalizes the GEE maximization task of the multi-LEO network. From the SINR (1), the achievable rate of GAP k on spot beam m of satellite s based on (1)-(3) is calculated as

$$R_{k,m,s} = \log_2 (1 + \gamma_{k,m,s}). \tag{8}$$

By taking the binary beam assignment indicator $x_{k,m,s}$ into account, the sum-rate can be written by

$$R = \sum_{s=1}^{S} \sum_{m=1}^{M} \sum_{k=1}^{K} R_{k,m,s} x_{k,m,s}. \tag{9}$$

We adopt the power consumption model from [17]-[20] in which both static and dynamic components are considered. Concretely, static power consumption Pcircuit,s of satellite s is drawn even when the satellite is not actively transmitting data, often due to leakage

currents and bias voltages within the circuitry. It is influenced by factors such as device technology, chip design, and operating conditions[21]. On top of that, dynamic power consumption occurs during active operations such as signal processing, modulation, and transmission. It is typically modelled to be proportional to the number of activated beams and a significant contributor to overall energy consumption[22]. This leads to the total power consumption of satellite s as

$$P_{\text{total},s} = \underbrace{P_{\text{circuit},s}}_{\text{static}} + \underbrace{\frac{1}{\rho_s}\sum_{m=1}^{M}\sum_{k=1}^{K} P_{k,m,s}x_{k,m,s}}_{\text{dynamic}}, \tag{10}$$

where $\rho_s \in (0, 1]$ indicates the efficiency of power conversion on satellite s.

Based on (8)-(10), the GEE η is defined as the ratio of the sum-rate to the total power consumption of all satellites, which can be expressed by

$$\eta = \frac{\sum_{s=1}^{S}\sum_{m=1}^{M}\sum_{k=1}^{K} R_{k,m,s}x_{k,m,s}}{\sum_{s=1}^{S}\left(P_{\text{circuit},s} + \frac{1}{\rho_s}\sum_{m=1}^{M}\sum_{k=1}^{K} P_{k,m,s}x_{k,m,s}\right)}. \tag{11}$$

Our objective is to maximize the GEE by optimizing the spot beam power allocation variables $\{P_{k,m,s}\}$ for given GAP-beam-satellite assignment $\{x_{k,m,s}\}$. The corresponding optimization task can be formulated as

$$\text{(P1)}: \max_{\{P_{k,m,s}\}} \ \eta \tag{12a}$$

$$\text{subject to:} \sum_{m=1}^{M}\sum_{k=1}^{K} P_{k,m,s}x_{k,m,s} \le \bar{P}_{\text{sat},s}, \forall s, \tag{12b}$$

$$\sum_{k=1}^{K} P_{k,m,s}x_{k,m,s} \le \bar{P}_{m,s}, \forall m, s, \tag{12c}$$

$$\text{TNI}_b \le \text{TNI}_{\max}, \forall b = 1, \ldots, B, \tag{12d}$$

where TNI_b stands for the terrestrial network interference towards GBS b, defined as

$$\text{TNI}_b = G_{\text{BS},b}\sum_{s=1}^{S} L_{b,s}\sum_{m=1}^{M} G_{\text{side},b,m,s}\sum_{k=1}^{K} P_{k,m,s}x_{k,m,s}, \tag{13}$$

Constraint (12b) ensures that the total spot beam power of satellite s does not exceed its power budget $\bar{P}_{\text{sat},s}$, and (12c) limits the power allocated to spot beam m of satellite s by the peak beam power constraint $\bar{P}_{m,s}$. Also, constraint (12d) guarantees the terrestrial network interference for every GBS is under the maximum allowable level $\text{TNI}_{\max}$.

It can be shown that the objective function in (P1) is non-convex with respect to the spot beam power variables, mainly due to mutual coupling in a complicated way. In the subsequent section, we first reformulate the problem into a more tractable form and then propose efficient optimization strategies.

Ⅳ. Proposed Solutions

4.1 Problem Reformulation

This section presents solution approaches for addressing the non-convex GEE maximization problem in (P1). To this end, we first simplify it by applying the change of variables. Without loss of generality, we rearrange the indices of all spot beams as an integer set $\mathcal{M} = [1, SM]$, where $[a, b] \triangleq \{a, a+1, \ldots, b-1, b\}$ indicates a set of integers between a and b. Then, the spot beams of satellite s can be represented by a set $\mathcal{M}_s \triangleq [(s-1)M+1, sM] \subset \mathcal{M}$. As a result, the power allocation variables $\{P_{k,m,s}\}$ and the constants $\{x_{k,m,s}\}$ can be equivalently converted into $\{P_{k,\tilde{m}}\}$ and $\{x_{k,\tilde{m}}\}$, which are respectively defined as

$$\begin{aligned} P_{k,\tilde{m}} &\triangleq P_{k,\tilde{m}-(s-1)M,s}, \forall \tilde{m} \in \mathcal{M}_s, s = 1, \ldots, S \\ &= P_{k,\tilde{m}-\left(\lceil \frac{\tilde{m}}{M} \rceil - 1\right)M,\lceil \frac{\tilde{m}}{M} \rceil}, \forall \tilde{m} \in \mathcal{M}, \end{aligned} \tag{14}$$

$$\begin{aligned} x_{k,\tilde{m}} &\triangleq x_{k,\tilde{m}-(s-1)M,s}, \forall \tilde{m} \in \mathcal{M}_s, s = 1, \ldots, S \\ &= x_{k,\tilde{m}-\left(\lceil \frac{\tilde{m}}{M} \rceil - 1\right)M,\lceil \frac{\tilde{m}}{M} \rceil}, \forall \tilde{m} \in \mathcal{M}. \end{aligned} \tag{15}$$

It is worth noting that the new index $\tilde{m}$ ranges from 1 to SM, and it virtually combines the multiple satellites into a single satellite projecting at most S groups of M beams. Similarly, we can newly define the following quantities:

$$\begin{aligned} \bar{P}_{\tilde{m}} &\triangleq \bar{P}_{\tilde{m}-(s-1)M,s}, \forall \tilde{m} \in \mathcal{M}_s \text{ and } s = 1, \ldots, S \\ &= \bar{P}_{\tilde{m}-\left(\lceil \frac{\tilde{m}}{M} \rceil - 1\right)M,\lceil \frac{\tilde{m}}{M} \rceil}, \forall \tilde{m} \in \mathcal{M}, \end{aligned} \tag{16}$$

$$\tilde{L}_{k,\tilde{m}} \triangleq L_{k,s}, \forall \tilde{m} \in \mathcal{M}_s \text{ and } s = 1,\ldots,S = L_{k,\lceil \frac{\tilde{m}}{M} \rceil}, \forall \tilde{m} \in \mathcal{M}, \tag{17}$$

$$\tilde{L}_{b,\tilde{m}} \triangleq L_{b,s}, \forall \tilde{m} \in \mathcal{M}_s \text{ and } s = 1,\ldots,S = L_{b,\lceil \frac{\tilde{m}}{M} \rceil}, \forall \tilde{m} \in \mathcal{M}, \tag{18}$$

$$\tilde{G}_{\text{main},\tilde{m}} \triangleq G_{\text{main},s}, \forall \tilde{m} \in \mathcal{M}_s \text{ and } s = 1,\ldots,S = G_{\text{main},\lceil \frac{\tilde{m}}{M} \rceil}, \forall \tilde{m} \in \mathcal{M}, \tag{19}$$

$$\tilde{G}_{\text{side},k,\tilde{m}} \triangleq \tilde{G}_{\text{side},k,\tilde{m}-(s-1)M,s}, \forall \tilde{m} \in \mathcal{M}_s, s = 1,\ldots,S = \tilde{G}_{\text{side},k,\tilde{m}-\left(\lceil \frac{\tilde{m}}{M} \rceil - 1\right)M,\lceil \frac{\tilde{m}}{M} \rceil}, \forall \tilde{m} \in \mathcal{M}, \tag{20}$$

$$\tilde{G}_{\text{side},b,\tilde{m}} \triangleq \tilde{G}_{\text{side},b,\tilde{m}-(s-1)M,s}, \forall \tilde{m} \in \mathcal{M}_s, s = 1,\ldots,S = \tilde{G}_{\text{side},b,\tilde{m}-\left(\lceil \frac{\tilde{m}}{M} \rceil - 1\right)M,\lceil \frac{\tilde{m}}{M} \rceil}, \forall \tilde{m} \in \mathcal{M}, \tag{21}$$

$$\tilde{f}_{k,\tilde{m}} \triangleq f_{k,s}, \forall \tilde{m} \in \mathcal{M}_s \text{ and } s = 1,\ldots,S = f_{k,\lceil \frac{\tilde{m}}{M} \rceil}, \forall \tilde{m} \in \mathcal{M}, \tag{22}$$

$$\tilde{\rho}_{\tilde{m}} \triangleq \rho_s, \forall \tilde{m} \in \mathcal{M}_s \text{ and } s = 1,\ldots,S = \rho_{\lceil \frac{\tilde{m}}{M} \rceil}, \forall \tilde{m} \in \mathcal{M}. \tag{23}$$

We next re-express the (P1) in terms of (14)-(23) as

$$\text{(P2)}: \max_{\{P_{k,\tilde{m}}\}} \ \eta \tag{24a}$$

$$\text{subject to:} \sum_{\tilde{m} \in \mathcal{M}_s} \sum_{k=1}^{K} P_{k,\tilde{m}} \le \bar{P}_{\text{sat},s}, \forall s, \tag{24b}$$

$$\sum_{k=1}^{K} P_{k,\tilde{m}} \le \bar{P}_{\tilde{m}}, \forall \tilde{m}, \tag{24c}$$

$$\text{TNI}_b \le \text{TNI}_{\max}, \forall b = 1,\ldots,B, \tag{24d}$$

with modified η and TNI_b as

$$\eta = \frac{\sum_{\tilde{m}=1}^{SM} \sum_{k=1}^{K} R_{k,\tilde{m}} x_{k,\tilde{m}}}{\sum_{s=1}^{S} \left(P_{\text{circuit},s} + \sum_{\tilde{m} \in \mathcal{M}_s} \frac{1}{\tilde{\rho}_{\tilde{m}}} \sum_{k=1}^{K} P_{k,\tilde{m}} x_{k,\tilde{m}} \right)}, \tag{25}$$

$$\text{TNI}_b = G_{\text{BS},b} \sum_{\tilde{m}=1}^{SM} \tilde{L}_{b,\tilde{m}} \tilde{G}_{\text{side},b,\tilde{m}} \sum_{k=1}^{K} P_{k,\tilde{m}} x_{k,\tilde{m}}, \tag{26}$$

where

$$\text{IBI}_{k,\tilde{m}} = G_{\text{AP},k} \sum_{\tilde{m}' \neq \tilde{m}} \sum_{k' \neq k} \tilde{L}_{k,\tilde{m}'} \tilde{G}_{\text{side},k,\tilde{m}'} P_{k',\tilde{m}'} x_{k',\tilde{m}'}, \tag{27}$$

$$\text{ICI}_{k,\tilde{m}} = G_{\text{AP},k} \tilde{L}_{k,\tilde{m}} \tilde{G}_{\text{main},\tilde{m}} P_{k,\tilde{m}} \left(1 - \text{sinc}^2\left(\tilde{f}_{k,\tilde{m}} T_{\text{sym}}\right)\right), \tag{28}$$

$$\gamma_{k,\tilde{m}} = \frac{G_{\text{AP},k} \tilde{L}_{k,\tilde{m}} \tilde{G}_{\text{main},\tilde{m}} P_{k,\tilde{m}}}{\text{IBI}_{k,\tilde{m}} + \text{ICI}_{k,\tilde{m}} + \sigma_{z,k}^2}, \tag{29}$$

$$R_{k,\tilde{m}} = \log_2\left(1 + \gamma_{k,\tilde{m}}\right). \tag{30}$$

Furthermore, since GAP k is paired with a unique and exclusive spot beam $\tilde{m}$, we can define the effective spot beam power as

$$P_{\tilde{m}} \triangleq \sum_{k=1}^{K} P_{k,\tilde{m}} = \sum_{k=1}^{K} P_{k,\tilde{m}} x_{k,\tilde{m}}. \tag{31}$$

Also, let $\mathcal{A} \triangleq \{(k,\tilde{m}) | x_{k,\tilde{m}} = 1, \forall k, \tilde{m}\}$ and $\mathcal{A}_{\text{beam}} \triangleq \{\tilde{m} | x_{k,\tilde{m}} = 1, \forall k, \tilde{m}\}$ be the sets of active GAP-spot beam pairs and active spot beams, respectively. Consequently, (25)-(29) can be further simplified into

$$\eta = \frac{\sum_{(k,\tilde{m}) \in \mathcal{A}} R_{k,\tilde{m}}}{\sum_{s=1}^{S} P_{\text{circuit},s} + \sum_{\tilde{m} \in \mathcal{A}_{\text{beam}}} \frac{1}{\tilde{\rho}_{\tilde{m}}} P_{\tilde{m}}}, \tag{32}$$

$$\text{TNI}_b = G_{\text{BS},b} \sum_{\tilde{m} \in \mathcal{A}_{\text{beam}}} \tilde{L}_{b,\tilde{m}} \tilde{G}_{\text{side},b,\tilde{m}} P_{\tilde{m}}, \tag{33}$$

$$\text{IBI}_{k,\tilde{m}} = G_{\text{AP},k} \sum_{\tilde{m}' \in \mathcal{A}_{\text{beam}}, \tilde{m}' \neq \tilde{m}} \tilde{L}_{k,\tilde{m}'} \tilde{G}_{\text{side},k,\tilde{m}'} P_{\tilde{m}'}, \tag{34}$$

$$\text{ICI}_{k,\tilde{m}} = G_{\text{AP},k} \tilde{L}_{k,\tilde{m}} \tilde{G}_{\text{main},\tilde{m}} P_{\tilde{m}} \left(1 - \text{sinc}^2\left(\tilde{f}_{k,\tilde{m}} T_{\text{sym}}\right)\right), \tag{35}$$

$$\gamma_{k,\tilde{m}} = \frac{G_{\text{AP},k} \tilde{L}_{k,\tilde{m}} \tilde{G}_{\text{main},\tilde{m}} P_{\tilde{m}}}{\text{IBI}_{k,\tilde{m}} + \text{ICI}_{k,\tilde{m}} + \sigma_{z,k}^2}. \tag{36}$$

Based on these results, (P2) can be equivalently transformed as

$$\text{(P3)}: \max_{\{P_{\tilde{m}} | \tilde{m} \in \mathcal{A}_{\text{beam}}\}} \ \eta, \tag{37a}$$

$$\text{subject to:} \sum_{\tilde{m} \in \mathcal{A}_{\text{beam}} \cap \mathcal{M}_s} P_{\tilde{m}} \le \bar{P}_{\text{sat},s}, \forall s, \tag{37b}$$

$$P_{\tilde{m}} \le \bar{P}_{\tilde{m}}, \forall \tilde{m} \in \mathcal{A}_{\text{beam}}, \tag{37c}$$

$$\text{TNI}_b \le \text{TNI}_{\max}, \forall b = 1,\ldots,B. \tag{37d}$$

Compared to (P1) which consists of KMS optimization variables $\{P_{k,m,s}\}$, (P3) now contains $|\mathcal{A}_{\text{beam}}| = \min(KS, MS) < KMS$ variables, thereby reducing the problem

complexity. Still, however, (P3) invokes the non-convex fractional form in the objective function (37a). Therefore, it is highly difficult to identify the globally optimal solution to (P3) using off-the-shelf convex optimization software.

4.2 Proposed Algorithm

We propose an efficient optimization algorithm that tackles the non-convexity of (P3). We first reformulate it by introducing an auxiliary variable λ as

$$\text{(P4)}: \max_{\{P_{\tilde{m}}|\tilde{m}\in\mathscr{A}_{\text{beam}}\},\lambda} \lambda, \tag{38a}$$

subject to:

$$\sum_{(k,\tilde{m})\in\mathscr{A}} R_{k,\tilde{m}} - \lambda\left(\sum_{s=1}^{S} P_{\text{circuit},s} + \sum_{\tilde{m}\in\mathscr{A}_{\text{beam}}} \frac{1}{\tilde{\rho}_{\tilde{m}}} P_{\tilde{m}}\right) \geq 0, \tag{38b}$$

$$\sum_{\tilde{m}\in\mathscr{A}_{\text{beam}}\cap\mathscr{M}_s} P_{\tilde{m}} \leq \bar{P}_{\text{sat},s}, \forall s, \tag{38c}$$

$$P_{\tilde{m}} \leq \bar{P}_{\tilde{m}}, \forall \tilde{m} \in \mathscr{A}_{\text{beam}}, \tag{38d}$$

$$\text{TNI}_b \leq \text{TNI}_{\max}, \forall b = 1,\ldots,B. \tag{38e}$$

It is readily seen that any $\lambda \in [0, \hat{\lambda}]$ is feasible for any feasible $\hat{\lambda}$ for (P4). This enables the use a two-layer optimization approach, in which an optimal $\lambda^\star$ for (P4) is found by the bisection method in the outer layer, while a feasible set of $\{P_{\tilde{m}}|\tilde{m}\in\mathscr{A}_{\text{beam}}\}$ is identified with each fixed λ in the inner layer.

It is not difficult to see that the feasible set $\{P_{\tilde{m}}|\tilde{m}\in\mathscr{A}_{\text{beam}}\}$ can be attained by determining the maximum of the left-hand side of constraint (38b). Therefore, in the inner layer, we solve the following optimization problem for a given λ :

(P4-inner):

$$\max_{\{P_{\tilde{m}}|\tilde{m}\in\mathscr{A}_{\text{beam}}\}} \sum_{(k,\tilde{m})\in\mathscr{A}} R_{k,\tilde{m}} - \lambda\left(\sum_{s=1}^{S} P_{\text{circuit},s} + \sum_{\tilde{m}\in\mathscr{A}_{\text{beam}}} \frac{1}{\tilde{\rho}_{\tilde{m}}} P_{\tilde{m}}\right), \tag{39a}$$

subject to:

$$\sum_{\tilde{m}\in\mathscr{A}_{\text{beam}}\cap\mathscr{M}_s} P_{\tilde{m}} \leq \bar{P}_{\text{sat},s}, \forall s, \tag{39b}$$

$$P_{\tilde{m}} \leq \bar{P}_{\tilde{m}}, \forall \tilde{m} \in \mathscr{A}_{\text{beam}}, \tag{39c}$$

$$\text{TNI}_b \leq \text{TNI}_{\max}, \forall b = 1,\ldots,B. \tag{39d}$$

The existence of feasible $\{P_{\tilde{m}}|\tilde{m}\in\mathscr{A}_{\text{beam}}\}$ for a certain λ is easily determined if the optimal value of (P4-inner) is greater than or equal to 0. Otherwise, it indicates that λ should be decreased in the outer bisection layer.

Unfortunately, the log-minus-log form of $R_{k,\tilde{m}}$ with respect to $\{P_{\tilde{m}}|\tilde{m}\in\mathscr{A}_{\text{beam}}\}$ in (39a) exhibits non-convexity, making (P4-inner) difficult to handle in the current form. Hence, we resort to the SCA technique which iteratively addresses convex-approximated tasks of the original formulation (P4-inner)[23]. Let us define the solution vector $\mathbf{p}$ and a function $g_{l,\tilde{m}}(\mathbf{p})$ as

$$\mathbf{p} \triangleq \left[P_{\tilde{m}_{\min}} \cdots P_{\tilde{m}_{\max}}\right]^T, \tag{40}$$

$$g_{k,\tilde{m}}(\mathbf{p}) \triangleq \log_2\left(\text{IBI}_{k,\tilde{m}} + \text{ICI}_{k,\tilde{m}} + \sigma_{z,k}^2\right), \tag{41}$$

with $\tilde{m}_{\min} \triangleq \min_{\tilde{m}\in\mathscr{A}_{\text{beam}}} \tilde{m}$ and $\tilde{m}_{\max} \triangleq \max_{\tilde{m}\in\mathscr{A}_{\text{beam}}} \tilde{m}$. According to the first-order Taylor expansion, an approximated convex expression of $R_{k,\tilde{m}}$ at a given solution $\mathbf{p}_0$ can be written by

$$\begin{aligned} R_{k,\tilde{m}} &= \log_2\left(G_{\text{AP},k}\tilde{L}_{k,\tilde{m}}\tilde{G}_{\text{main},\tilde{m}}P_{\tilde{m}} + \text{IBI}_{k,\tilde{m}} + \text{ICI}_{k,\tilde{m}} + \sigma_{z,k}^2\right) \\ &\quad - g_{k,\tilde{m}}(\mathbf{p}) \\ &\simeq \log_2\left(G_{\text{AP},k}\tilde{L}_{k,\tilde{m}}\tilde{G}_{\text{main},\tilde{m}}P_{\tilde{m}} + \text{IBI}_{k,\tilde{m}} + \text{ICI}_{k,\tilde{m}} + \sigma_{z,k}^2\right) \\ &\quad - \left(g_{k,\tilde{m}}(\mathbf{p}_0) + \text{vec}\left(\frac{\partial g_{k,\tilde{m}}(\mathbf{p})}{\partial \mathbf{p}}\bigg|_{\mathbf{p}=\mathbf{p}_0}\right)^T(\mathbf{p}-\mathbf{p}_0)\right), \\ &\triangleq \tilde{R}_{k,\tilde{m}}. \end{aligned} \tag{42}$$

As a consequence, the convex approximated inner layerproblem (P4-inner) is formulated as

(P4-inner-SCA):

$$\max_{\{P_{\tilde{m}}|\tilde{m}\in\mathscr{A}_{\text{beam}}\}} \sum_{(k,\tilde{m})\in\mathscr{A}} \tilde{R}_{k,\tilde{m}} - \lambda\left(\sum_{s=1}^{S} P_{\text{circuit},s} + \sum_{\tilde{m}\in\mathscr{A}_{\text{beam}}} \frac{1}{\tilde{\rho}_{\tilde{m}}} P_{\tilde{m}}\right) \tag{43a}$$

subject to:

$$\sum_{\tilde{m}\in\mathscr{A}_{\text{beam}}\cap\mathscr{M}_s} P_{\tilde{m}} \leq \bar{P}_{\text{sat},s}, \forall s, \tag{43b}$$

$$P_{\tilde{m}} \leq \bar{P}_{\tilde{m}}, \forall \tilde{m} \in \mathscr{A}_{\text{beam}}, \tag{43c}$$

$$\text{TNI}_b \leq \text{TNI}_{\max}, \forall b = 1,\ldots,B. \tag{43d}$$

Problem (P4-inner-SCA) now becomes convex, which can be easily tackled using existing convex solvers, e.g., CVXPY[24].

We summarize the proposed spot beam power allocation algorithm in Algorithm 1. As discussed, the overall procedure consists of the outer layer for obtaining λ using the bisection method and the inner layer addressing (P4-inner) using the SCA algorithm.

We first initialize the power allocation solution $\mathbf{p}_0$ and the bound of $\lambda \in [\lambda_{LB}, \lambda_{UB}]$. Also, we set the tolerance δ and the number of maximum iterations of the inner layer I_{max}. At each iteration of the outer layer, a new λ is set to the median of the predetermined bound as $\lambda \leftarrow \frac{\lambda_{LB}+\lambda_{UB}}{2}$. Then, the SCA algorithm is adopted which solves (P4-inner-SCA) repeatedly. Denoting $\tilde{\eta}$ as the optimal value of (P4-inner-SCA) at the convergence, the bisection method is employed to update the lower and upper bounds of λ. Such a procedure is repeated until λ converges within the predefined tolerance δ.

Algorithm 1 Spot Beam Power Optimization

Initialize $\mathbf{p}_0 \leftarrow \mathbf{0}$, $\lambda_{LB} \leftarrow 0$, $\lambda_{UB} \gg 1$.
Set $\delta \ll 1$ and integer ℓ_{max}.
while $|\lambda_{UB} - \lambda_{LB}| < \delta$ **do**
  Set $\lambda \leftarrow \frac{\lambda_{LB}+\lambda_{UB}}{2}$.
  for $\ell = 1, \ldots, \ell_{max}$ **do**
    Obtain the solution $\mathbf{p}^\star$ of (P4-inner-SCA) for given $\mathbf{p}_0$ and λ.
    Set $\mathbf{p}_0 \leftarrow \mathbf{p}^\star$.
  end for
  if $\tilde{\eta} \geq 0$ **then**
    Set $\lambda_{LB} \leftarrow \lambda$.
  else
    Set $\lambda_{UB} \leftarrow \lambda$.
  end if
end while

Ⅴ. Numerical Results

We evaluate the proposed spot beam power optimization algorithm through numerical simulations. We incorporate the rain fading model for satellite-to-ground links as specified in [25], [26]. Thus, the small- scale fading component between ground node X and satellite s is modeled as

$$\tilde{h}_{X,s} = \sqrt{\xi}\exp(-j\phi), \tag{44}$$

where ξ denotes the small-scale channel gain whose dB scale value $\xi_{dB} = 20\log_{10}(\xi)$ follows the log-normal distribution with mean μ and variance σ^2, i.e., $\ln(\xi_{dB}) \sim \mathcal{N}(\mu, \sigma)$, and $\phi \sim \mathcal{U}(0, 2\pi)$ stands for the random phase changes. Notice that the parameters μ and σ depend on environmental factors such as receiver location, operation frequency, polarization, and the elevation angle towards the satellite. The overall channel attenuation, denoted by $L_{X,s}$, is then calculated as [12]

$$L_{X,s} = \left(\frac{c}{4\pi f_c d_{Xs}}\right)^2 |\tilde{h}_k|^2, \tag{45}$$

where d_{Xs} indicates the distance between ground node X and satellite s.

We adopt the satellite antenna gain model described in ITU-R S.672-4 as

$$G_{sat}(\theta_{X,m,s}) = \begin{cases} \bar{G}_{sat,m,s}, & \text{if } \theta_{X,m,s} \leq \bar{\theta}_{m,s}, \\ \bar{G}_{sat,m,s} - 3\left(\frac{\theta_{X,m,s}}{\bar{\theta}_{m,s}}\right)^{\alpha}, & \text{if } \bar{\theta}_{m,s} < \theta_{X,m,s} \leq a\bar{\theta}_{m,s}, \\ \bar{G}_{sat,m,s} + \Psi, & \text{if } a\bar{\theta}_{m,s} < \theta_{X,m,s} \leq b\bar{\theta}_{m,s}, \\ \bar{G}_{sat,m,s} + \Psi + 20 & \\ \quad -25\log_{10}\left(\frac{\theta_{X,m,s}}{\bar{\theta}_{m,s}}\right), & \text{if } b\bar{\theta}_{m,s} < \theta_{X,m,s} \leq \check{\theta}_{m,s}, \\ 0, & \text{if } \check{\theta}_{m,s} < \theta_{X,m,s}, \end{cases} \tag{46}$$

in dBi where $\theta_{X,m,s}$ indicates the angle between ground node X and the direction of beam m from satellite s, $\bar{G}_{sat,m,s}$ denotes the maximum main lobe gain of beam m at satellite s, $\bar{\theta}_{m,s}$ signifies the angle at which the gain falls 3 dB below the maximum, $\check{\theta}_{m,s}$ marks the angle at which the third equation in (46) becomes 0 dBi, and Ψ determines the required near-in-side-lobe level relative to peak gain[27]. In this work, we set $\alpha = 2$ $a = 2.58$, $b = 6.32$, $\Psi = -20$, $G_{main,s} = \bar{G}_{sat,m,s}$ $\forall m, s$[25], $G_{side,X,m,s} = G_{sat}(\theta_{X,m,s})$, $\forall X, m, s$, and $\bar{\theta}_{X,m} = 0.5^\circ$, $\forall X, m$[28].

It is assumed that K_s ground terminals are randomly located within a horizontal range of $d_{X,s}$ from satellite s. The satellites are positioned in a circular formation with radius r_s from the origin, each separated by angle $\theta_s = 2\pi/S$. System parameters are set as outlined in Table 1, unless otherwise stated. Fig. 2 illustrates an example of node placement when $K_s = 10$, $B = 10$, and $S = 3$.

Table 1. System setup

Parameter	Setting	Parameter	Setting
B	28 MHz	f_c	20 GHz
T_{sym}	1 μs	h	780 km
v_s	7.46 km/s	S	3
K_s	10	B	10
M	K_s	d_{Xs}	2500 km
$\bar{G}_{\mathrm{sat},m,s}$	52.1 dB	$G_{\mathrm{side,X,m,s}}$	G_{sat} $(\theta^{X,m,s})$ dBi
$G_{\mathrm{BS},b}$	5 dB	$G_{\mathrm{AP,k}}$	U(10, 15) dB
$\bar{P}_{m,s}$	20 dBW	$\bar{P}_{\mathrm{sat},s}$	20 dBW
$\mathrm{TNI}_{\max}$	-111 dB	$P_{\mathrm{circuit},s}$	10 dBW
ρ_s	0.8	$\sigma^2_{z,k}$	−174 dBW/Hz
μ	-2.6 dB	σ	1.6 dB
r_s	2500 km	θ_s	2π/S

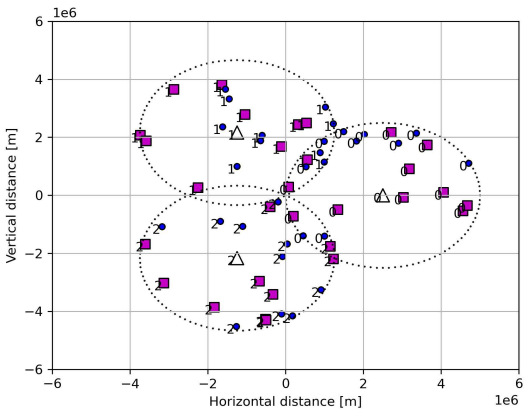

Fig. 2. An example of node placement with K_s = 10 (○), B = 10 (□), and S = 3 (△) where the numeric marker indicates the associated satellite index

For comparison, we consider the following baseline methods that address the inner layer problem (P4-inner).

- *Sequential least squares programming* (*SLSQP*)[29]: This method solves a sequence of quadratic subproblems to handle nonlinear optimization problems with both equality and inequality constraints.
- *Trust-region algorithm for constrained optimization* (*Trust-constr*)[30]: We leverage a trust- region interior point approach, introducing slack variables and solving a sequence of equality- constrained barrier problems with decreasing barrier parameters.
- *Equal power allocation* (*EPA*)[15]: From (24b)-(24d), we consider the following equally distributed power allocation as

$$P_{\tilde{m}} = \min\left\{ \frac{\min_s \bar{P}_{\mathrm{sat},s}}{M}, \min_{\tilde{m}} \bar{P}_{\tilde{m}}, \frac{\mathrm{TNI}_{\max}}{\left(\max_b G_{\mathrm{BS},b}\right)\left(\max_{\tilde{m}} \tilde{L}_{b,\tilde{m}} \tilde{G}_{\mathrm{side},b,\tilde{m}}\right) SM} \right\}, \forall \tilde{m}, \tag{47}$$

which can be verified to be always feasible.

Fig. 3 shows the average GEE as a function of the number of satellites S for different number of GAPs per satellite Ks with random spot beam-GAP assignment. The proposed SCA-based algorithm clearly out- performs the baseline algorithms for all S and Ks . We also observe that the GEE generally improves with higher S in most schemes except for the equal power allocation (EPA) strategy. This implies that the adjustment of spot beam power becomes even more important when there are more number of satellites. The figure also shows that the GEE increases with Ks for every scheme. This performance gain stems from the increased diversity in the channel links.

Fig. 4 compares the average GEE in terms of the number of GAPs per satellite Ks with different number of satellites S. We first note that the proposed SCA method provides the highest η across all values of S and Ks , which emphasizes the effectiveness over other algorithms. While the GEE of the schemes that optimize the spot beam power increases for different S, it is the opposite for the EPA strategy. This is in

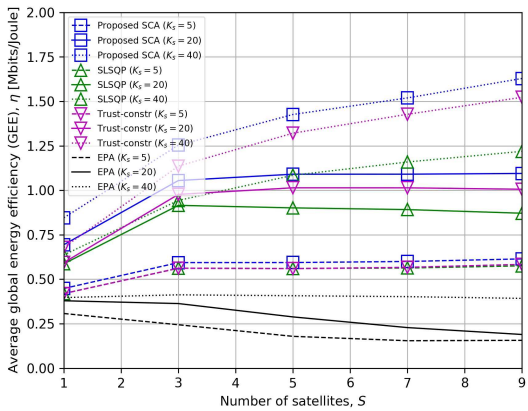

Fig. 3. GEE versus the number of satellites

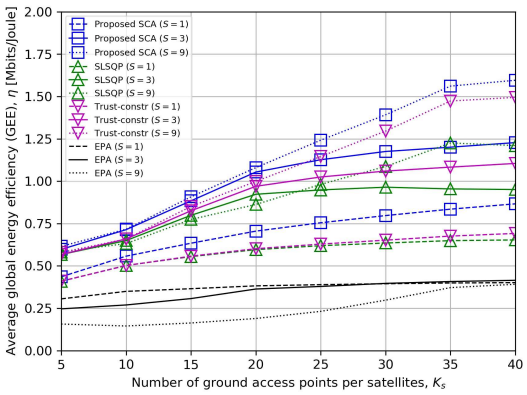

Fig. 4. GEE versus the number of GAPs per satellite

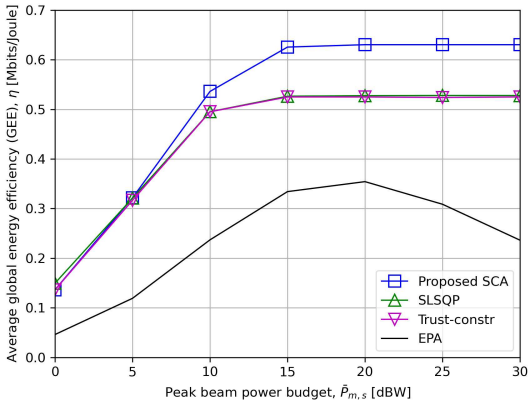

Fig. 6. GEE versus the peak beam power of satellites

line with our interpretation in Fig. 3.

Fig. 5 compares the average GEE performance by varying the maximum main lobe gain $\bar{G}_{\mathrm{sat},m,s}$. The GEE of all schemes gradually increases as $\bar{G}_{\mathrm{sat},m,s}$ grows since the desired signal power gets larger. The proposed SCA method outperforms other benchmark schemes regardless of $\bar{G}_{\mathrm{sat},m,s}$. The gain is particularly significant in the high main lobe gain regime, where the interference management becomes more important. Thus, it can be concluded that the proposed approach is efficient in handling interference through optimized power allocation strategies.

Fig. 6 examines the average GEE with respect to the power budget $\bar{P}_{\mathrm{sat},s} = \bar{P}_{m,s}$. We can first see that the proposed SCA exhibits the highest GEE performance compared to benchmark schemes. The optimization- based schemes including the SCA, SLSQP, and Trust- constr converge to specific GEE values as the transmit power gets larger. This is because the increase in the IBI and ICI limits the sum-rate per unit power consumption. Therefore, in terms of the GEE performance, it is beneficial not to exhaust all the available power budget. Since the EPA always utilizes the total power constraint, its GEE performance decreases after a certain power. This demonstrates the necessity of the power control algorithms for maximizing the GEE in the multi-LEO satellite networks.

Fig. 7 presents the average GEE with respect to the static circuit power $P_{\mathrm{circuit},s}$. It is clear that the GEE monotonically decreases with $P_{\mathrm{circuit},s}$. The proposed SCA is superior to other baseline schemes, proving its effectiveness for arbitrary static circuit power consumption.

Fig. 8 investigates the average GEE as a function of the velocity of satellites *vs* . We observe that a

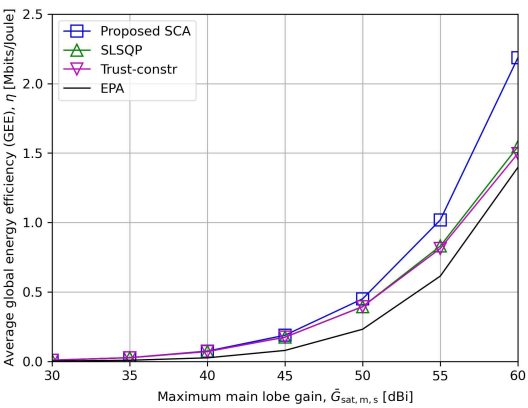

Fig. 5. GEE versus the maximum main lobe gain of beams at satellites

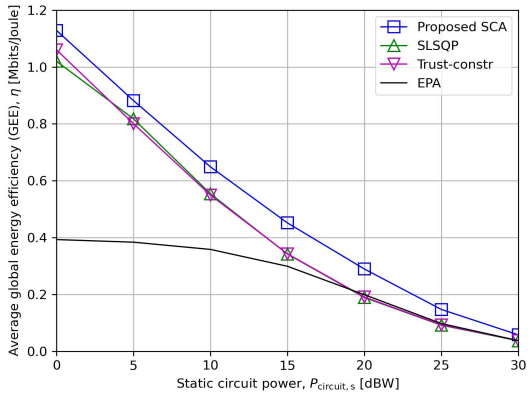

Fig. 7. GEE versus the static circuit power at satellites

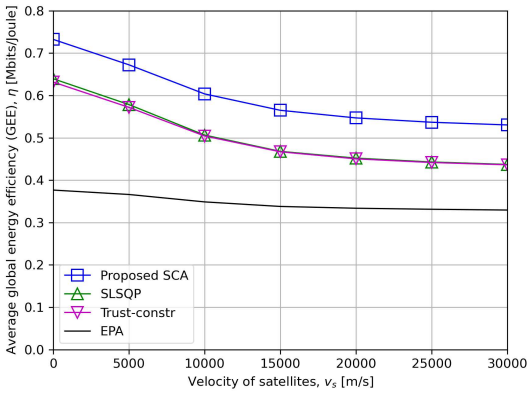

Fig. 8. GEE versus the velocity of satellites

faster movement of satellites degrades the GEE performance due to the increase in the ICI. Moreover, the proposed SCA algorithm outperforms all the other compared schemes. Thus, it is concluded that the proposed approach is effective for any given satellite mobility.

Ⅵ. Conclusion

In this paper, we studied a spot beam power control of multiple LEO satellites for downlink transmission. To be specific, we optimized the sum-rate and total power consumption to maximize the GEE of the satellites, each of which supports associated GAPs. We first formulated a GEE maximization problem taking all the inter-beam, inter-carrier, and terrestrial network interference into account. To ease the complexity of the problem, we further simplified the expressions of the GEE and interference and then proposed a SCA-based spot beam power optimization method. Numerical results validated its effectiveness over baseline algorithms in different system setups.

To further enhance the GEE performance, a joint optimization of GAP-beam-LEO satellite scheduling and spot beam power control can be an interesting extension. We can also delve into dynamic scenarios with temporal variations in GAP locations and service demands, which lead to imperfect and outdated channel state information at the satellites. Considering the load of inter-satellite link (ISL) message exchange and developing a decentralized control of multiple LEO satellites can also be a potential future work.

References

[1] J. Moon, "Hybrid DF/AF relay-based low-probability-of-detection satellite communications," in *2025 Winter Conf. KICS*, pp. 1-2, Feb. 2025.

[2] S.-C. Lin, C.-H. Lin, L. C. Chu, and S.-Y. Lien, "Enabling resilient access equality for 6G LEO satellite swarm networks," *IEEE Internet Things J.*, vol. 6, no. 3, pp. 38-43, Sep. 2023.

[3] D. G. Riviello, B. Ahmad, A. Guidotti, and A. Vanelli-Coralli, "Joint graph-based user scheduling and beamforming in LEO-MIMO satellite communication systems," in *2022 11th Advanced Satellite Multimedia Syst. Conf. and the 17th Signal Process. for Space Commun. Wkshp.* (*ASMS/SPSC*), pp. 1-8, Graz, Austria, Sep. 2022.

[4] S. Mahboob and L. Liu, "Revolutionizing future connectivity: A contemporary survey on AI-empowered satellite-based non-terrestrial networks in 6G," *IEEE Commun. Surv. Tuts.*, vol. 26, no. 2, pp. 1279-1321, Secondquarter 2024.

[5] M. A. Jamshed, A. Kaushik, M. Dajer, et al., "Non-terrestrial networks for 6G: Integrated, intelligent and ubiquitous connectivity," [Online] Available: https://arxiv.org/abs/2407.02184

[6] F. Wang, S. Zhang, H. Yang, and T. Q. S. Quek, "Non-terrestrial networking for 6G: Evolution, opportunities, and future directions," [Online] Available: https://arxiv.org/abs/2412.00820

[7] D. Wang, M. Giordani, M.-S. Alouini, and M. Zorzi, "The potential of multilayered hierarchical nonterrestrial networks for 6G: A comparative analysis among networking architectures," *IEEE Veh. Technol. Mag.*, vol. 16, no. 3, pp. 99-107, Sep. 2021.

[8] W. U. Khan, E. Lagunas, A. Mahmood, S. Chatzinotas, and B. Ottersten, "Energy-

efficient RIS-enabled NOMA communication for 6G LEO satellite networks," in *2023 IEEE 97th VTC2023- Spring*, pp. 1-6, Florence, Italy, Jun. 2023.

[9] C. Qi and X. Wang, "Precoding design for energy efficiency of multibeam satellite communications," *IEEE Commun. Lett.*, vol. 22, no. 9, pp. 1826-1829, Sep. 2018.

[10] C. Qi, Y. Yang, R. Ding, S. Jin, and D. Liu, "Multibeam satellite communications with energy efficiency optimization," *IEEE Commun. Lett.*, vol. 26, no. 4, pp. 887-891, Apr. 2022.

[11] S. S. Hassan, D. H. Kim, Y. K. Tun, N. H. Tran, W. Saad, and C. S. Hong, "Seamless and energy-efficient maritime coverage in coordinated 6G space-air-sea non-terrestrial networks," *IEEE Internet Things J.*, vol. 10, no. 6, pp. 4749-4769, Mar. 2023.

[12] Q. Liao and M. Kaneko, "Global energy efficiency optimization of a Ka-Band multi-beam LEO satellite communication system," *IEEE Access*, vol. 9, pp. 55232-55243, Apr. 2021.

[13] K. Lin, M. A. Ullah, H. Alves, K. Mikhaylov, and T. Hao, "Energy efficiency optimization for subterranean LoRaWAN using a reinforcement learning approach: A direct-to-satellite scenario," *IEEE Wireless Commun. Lett.*, vol. 13, no. 2, pp. 308-312, Feb. 2024.

[14] S. M. M. Shahabi, X. Deng, A. Qidan, T. Elgorashi, and J. Elmirghani, "Energy-efficient functional split in non-terrestrial open radio access networks," in *GLOBECOM 2024*, pp. 3799-3804, Cape Town, South Africa, Dec. 2024.

[15] J. Moon and H. Lee, "Energy efficiency maximization for multi-LEO satellite networks," in *2024 Fifteenth ICUFN*, pp. 1-5, Budapest, Hungary, Jul. 2024.

[16] T. 3. G. P. P. (3GPP), *TS 38.101-2: NR; User Equipment (UE) radio transmission and reception; Part 2: Range 2 Standalone*, Last accessed 11 Apr. 2025, 2025. [Online]. Available: https://portal.3gpp.org/desktopmodules/Specifications/SpecificationDetails.aspx?specificationId=3284

[17] S. Wu, Y. Wang, G. Sun, L. You, W. Wang, and R. Ding, "Energy and computational efficient precoding for LEO satellite communications," in *GLOBECOM 2023*, pp. 1872-1877, Kuala Lumpur, Malaysia, Dec. 2023.

[18] Q. Wang, X. Liang, H. Zhang, and L. Ge, "AoI-aware energy efficiency resource allocation for integrated satellite-terrestrial IoT networks," *IEEE Trans. Green Commun. Netw.*, vol. 9, no. 1, pp. 125-139, Mar. 2025.

[19] A. Zhou, Y. Wang, and Q. Zhang, "Energy-efficient resource management for federated learning in LEO satellite IoT," in *2024 IEEE WCNC*, pp. 1-6, Dubai, United Arab Emirates, Apr. 2024.

[20] J. Li, R. Chai, C. Liu, C. Liang, Q. Chen, and F. R. Yu, "Energy-aware joint route selection and resource allocation in heterogeneous satellite networks," *IEEE Trans. Veh. Technol.*, vol. 73, no. 8, pp. 12067-12081, Aug. 2024.

[21] J. Wang, W. Tang, S. Jin, X. Li, and M. Matthaiou, "Static power consumption modeling and measurement of reconfigurable intelligent surfaces," in *2023 31st EUSIPCO*, pp. 890-894, Helsinki, Finland, Sep. 2023.

[22] M. Sinaie, A. Zappone, E. A. Jorswieck, and P. Azmi, "A novel power consumption model for effective energy efficiency in wireless networks," *IEEE Wireless Commun. Lett.*, vol. 5, no. 2, pp. 152-155, Apr. 2016.

[23] A. Liu, V. K. N. Lau, and B. Kananian, "Stochastic successive convex approximation for non-convex constrained stochastic optimization," *IEEE Trans. Signal Process.*, vol. 67, no. 16, pp. 4189-4203, Aug. 2019.

[24] S. Diamond and S. Boyd, "CVXPY: A python-embedded modeling language for convex optimization," *J. Machine Learn. Res.*, vol. 17, no. 83, pp. 1-5, 2016.

[25] K. An, T. Liang, G. Zheng, X. Yan, Y. Li, and S. Chatzinotas, "Performance limits of cognitive-uplink FSS and terrestrial FS for Ka-band," *IEEE Trans. Aerosp. Electr. Syst.*, vol. 55, no. 5, pp. 2604-2611, Oct. 2019.

[26] I. T. U.-R. (ITU-R), *P.618 : Propagation data and prediction methods required for the design of Earth-space telecommunication systems*, Last accessed 21 Mar. 2024, 2023. [Online]. Available: https://www.itu.int/rec/R-REC-P.618/en

[27] I. T. U.-R. (ITU-R), *S.672-4 : Satellite antenna radiation pattern for use as a design objective in the fixed-satellite service employing geostation- ary satellites*, Last accessed 22 May 2025, 1997. [Online]. Available: https://www.itu.int/rec/R-REC-S.672-4-199709-I/en

[28] Avanti, *Ka vs Ku band HTS: A performance assessment and comparison of Ka vs Ku Band HTS*, Last accessed 23 May 2025, 2021. [Online]. Available: https://www.avanti.space/wp-content/uploads/2021/04/Avanti-White-Paper-Kavs-Ku-HTS.pdf

[29] Y. Ma, X. Gao, C. Liu, and J. Li, "Improved SQP and SLSQP algorithms for feasible path-based process optimisation," *Computers & Chemical Eng.*, vol. 188, no. 108751, Sep. 2024.

[30] S. J. Sadjadi and K. Ponnambalam, "Advances in trust region algorithms for constrained optimization," *Applied Numerical Mathematics*, vol. 29, no. 3, pp. 423-443, Mar. 1999.

Jihwan Moon

Feb. 2014 : B.Eng., Department of Electrical Engineering, Korea University, the Republic of Korea

Feb. 2019 : Ph.D., Department of Electrical Engineering, Korea University, the Republic of Korea

Feb. 2012 : B.S., Department of Electrical Engineering, Korea University, the Republic of Korea

Feb. 2017: Ph.D., Department of Electrical Engineering, the Republic of Korea

Jan. 2018~Mar. 2018 : Visiting research student, King's College London, the United Kingdom

Mar. 2019~Jul. 2019 : Postdoctoral research associate, Research Institute for Information and Communication Technology (RICT), Korea University, the Republic of Korea

Jul. 2019 ~Aug. 2020 : Researcher, The Affiliated Institute of Electronics and Telecommunications Research Institute (ETRI), the Republic of Korea

Sept. 2020~Feb. 2022 : Assistant professor, Department of Information and Communication Engineering, Chosun University, the Republic of Korea

Mar. 2022~Current : Assistant professor, Department of Mobile Convergence Engineering, Hanbat National University, the Republic of Korea

<Research Interest> Optimization techniques, energy harvesting, physical-layer security, wireless surveillance, covert communications, and machine learning for wireless communications.

[ORCID:0000-0002-9812-7768]

Hoon Lee

Mar. 2018~Feb. 2019 : Postdoc. Fellow, Singapore University of Technology and Design (SUTD), Singapore

Mar. 2019~Aug. 2022 : Assistant Professor, Pukyong National University, Busan, Korea

Sept. 2022~Aug. 2023 : Associate Professor, Pukyong National University, Busan, Korea

Sept. 2023~Current : Associate Professor, Ulsan National Institute of Science and Technology (UNIST), Ulsan, Korea

<Research Interest> Optimization, machine learning, and signal processing for wireless networks.

[ORCID:0000-0003-0753-8324]